

Parallel Comparative Studies on Mouse Toxicity of Oxide Nanoparticle- and Gadolinium-Based T1 MRI Contrast Agents

Rui Chen,^{†,#} Daishun Ling,^{*,‡,§,||,#} Lin Zhao,[†] Shuaifei Wang,[‡] Ying Liu,[†] Ru Bai,[†] Seungmin Baik,^{†,||} Yuliang Zhao,[†] Chunying Chen,^{*,†} and Taeghwan Hyeon^{*,†,||}

[†]CAS Key Lab for Biomedical Effects of Nanomaterials and Nanosafety, National Center for Nanoscience and Technology of China, Beijing 100190, P. R. China,

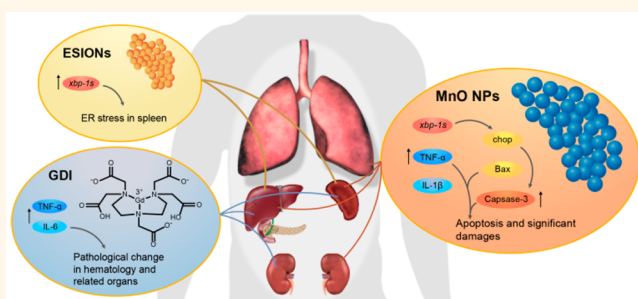
[‡]Zhejiang Province Key Laboratory of Anti-Cancer Drug Research, College of Pharmaceutical Sciences, Zhejiang University, Hangzhou 310058, P. R. China,

[§]Key Laboratory of Biomedical Engineering of the Ministry of Education, Zhejiang University, Hangzhou 310058, P. R. China, ^{||}Center for Nanoparticle

Research, Institute for Basic Science (IBS), Seoul 151-742, Korea, and ^{||}School of Chemical and Biological Engineering, Seoul National University,

Seoul 151-742, Korea. [#]These authors contributed equally to this work.

ABSTRACT Magnetic resonance imaging (MRI) contrast agents with high relaxivity are highly desirable because they can significantly increase the accuracy of diagnosis. However, they can be potentially toxic to the patients. In this study, using a mouse model, we investigate the toxic effects and subsequent tissue damage induced by three T1 MRI contrast agents: gadopentetate dimeglumine injection (GDI), a clinically used gadolinium (Gd)-based contrast agent (GBCAs), and oxide nanoparticle (NP)-based contrast agents, extremely small-sized iron oxide NPs (ESIONs) and manganese oxide (MnO) NPs. Biodistribution, hematological and histopathological changes, inflammation, and the endoplasmic reticulum (ER) stress responses are evaluated for 24 h after intravenous injection. These thorough assessments of the toxic and stress responses of these agents provide a panoramic description of safety concerns and underlying mechanisms of the toxicity of contrast agents in the body. We demonstrate that ESIONs exhibit fewer adverse effects than the MnO NPs and the clinically used GDI GBCAs, providing useful information on future applications of ESIONs as potentially safe MRI contrast agents.



KEYWORDS: magnetic resonance imaging · contrast agent · iron oxide nanoparticles · toxicity evaluation · endoplasmic reticulum stress · biodistribution

Magnetic resonance imaging (MRI) can provide detailed images of structural abnormalities and lesions in the body, which is further facilitated by the signal enhancing ability of contrast agents.^{1–4} Gadolinium (Gd)-based contrast agents (GBCAs) have been approved by the FDA and European agencies in the late 1980s, and have been widely used in clinical practice,⁵ although they have shown potential toxicities including the well-known nephrogenic systemic fibrosis (NSF).^{6–8} In addition to GBCAs, various inorganic nanoparticles (NPs) have been studied as MRI contrast agents owing to their unique properties such as efficient contrasting effect and large surface area.^{9–11} In particular,

uniform-sized oxide NPs, such as extremely small-sized iron oxide NPs (ESIONs)^{12,13} and manganese oxide (MnO) NPs,¹⁴ have demonstrated excellent T1 MRI contrast effects comparable to GBCA agents. For instance, in the previous studies, these NP-based contrast agents have overcome several drawbacks of GBCAs, enabling specific targeted imaging of tumor and blood pool imaging using a clinical 3 T scanner. On the basis of the present knowledge,^{15,16} the *in vivo* safety, not the MRI capability, is the main obstacle for the clinical applications of these new generation NP-based contrast agents.

Generally, PEGylation is a routine method used to minimize cytotoxicity and prolong the circulation time of NPs, thereby extending

* Address correspondence to
lingds@zju.edu.cn,
chenchy@nanoctr.cn,
thyeon@snu.ac.kr.

Received for review September 15, 2015
and accepted November 15, 2015.

Published online November 15, 2015
10.1021/acsnano.5b05783

© 2015 American Chemical Society

their half-life in the blood.¹⁷ Furthermore, the biocompatibility of the NPs can also be improved by this simple, time-saving, and low energy-consuming modification process.¹⁷ Although the long blood circulation of NP-based contrast agents has certain advantages for MRI, such as blood pool imaging, it also increases the chances of tissue-material interactions. Similar to GBCAs, ion leakage is inevitable even with these well-protected biocompatible NP-based contrast agents.¹⁸ Zinc and copper, which are normally present in small amounts in the bloodstream, have a competing affinity to displace gadolinium ions from the chelating molecule, and therefore, prolonged retention of GBCAs may increase the dissociation of gadolinium.⁸ Furthermore, biocompatibility does not necessarily equal safety, and the lack of evidence of acute toxicity and immunogenicity has prevented the approval for their clinical use. The requirements for the safety evaluation of the adverse health impacts are highly stringent and must be accompanied by supporting evidence of routine toxicological end points. The cellular viability, pathological staining and pharmacokinetic assays are generally used to evaluate the toxicity of nanomaterials.^{19–21} However, it is not easy for material scientists themselves who focusing on the MRI function to find out the subtle toxicity of their handled materials by these routine testing methods, much less to disclose the safety differences when comparing to clinical GBCAs.^{22–24} Highly sensitive assays should be developed to fulfill this task.²⁵

The U.S. Environmental Protection Agency (EPA) and the National Research Council (NRC) suggested that toxicity testing on cellular response or adverse outcome pathways (AOP) for adverse health effect evaluation should be the preferred toxicity testing strategy in the 21st century.^{26,27} *In vitro* AOP testing is a sensitive method that provides hazard identification ahead of realistic toxic effect generation on the basis of both time and dose lines. Therefore, we considered these factors in our previous research on the pathways of endoplasmic reticulum (ER) stress,^{28,29} which is also known as the unfolded protein response (UPR), and is a conserved cellular self-protection mechanism for monitoring the steady state of cell functions. It occurs rapidly when the concentration of outer stimuli exceeds the physiological threshold of cellular self-protection, and prolonged stress activates apoptotic cell death pathways.^{30–32} It was reported that free gadolinium ions cause toxicity by inducing the ER stress response pathway.^{33,34} The basic mechanism for stress initiation involves interruption of the activation of the calcium-sensing receptor (CaR)-mediated cellular calcium homeostasis, which may occur after binding of the activators by free ions such as Gd³⁺ and Mn²⁺.^{35,36} However, the discovery that *in vitro* and *in vivo* dose-response adverse effects are more meaningful for risk assessments suggests that identifying the potential hazards

alone is still insufficient for the assessment of contrast agents.^{28,37}

Various studies have investigated the toxic effects of different GBCAs and NPs using different methods.^{24,38,39} In this study, we used a mouse model to conduct a parallel comparison of the toxicity and ER stress-inducing ability of three T1 MRI contrast agents: the clinically used GBCAs, synthesized ESIONs, and MnO NPs at their current MRI application doses.¹⁶

RESULTS AND DISCUSSION

Characterization of MRI Contrast Agents. As shown in the transmission electron microscopy (TEM) images, both ESIONs and MnO NPs exhibit a narrow particle diameter distribution with sizes of about 3 and 15 nm, respectively (Figure 1A,B, insets, TEM images of high magnification observation). After PEGylation, these particles are both negatively charged in cell culture medium, -1 to approximately -3 mV, with hydrodynamic sizes of around 15 and 30 nm, respectively (Figure 1C,D, Table S1). They were both very stable in aqueous media as the polyethylene glycol (PEG) tail group endows the nanoparticles with colloidal stability (Figure S1). Moreover, they were both demonstrated to be excellent T1 contrast agents in the previously studies,^{13,14} while GD injection (GDI) is used in clinical imaging, and its molecular formula is provided in Figure S2.

Biodistribution of Contrast Agents Following Intravenous Administration at Doses Used in MRI Applications. Inductively coupled plasma-mass spectrometry (ICP-MS) was used to quantify the related metal elements in mouse tissue 24 h after a single tail vein injection. The clinical MRI dose of GDI is $0.2\text{ }\mu\text{mol/g}$, which is equivalent to about $30\text{ }\mu\text{g/g}$ (body weight) of Gd element. Three graded doses (low, medium, and high; 2, 5, and $10\text{ }\mu\text{g/g}$, respectively) were adopted for ESION and MnO NPs in order to compare their possible dose-toxicity responses, while ESION was used at a suitable dose of $2.5\text{ }\mu\text{g/g}$ for the *in vivo* MRI scanning.¹³ After exposure to the three contrast agents for 24 h, no significant changes were found in the body weight of the mice (Figure 2A). Furthermore, as we expected, the reticuloendothelial system related organs such as the liver and spleen captured most of the contrast agents with a correspondingly high level of the metal elements (Figure 2B–D). Captured foreign materials are usually cleared by macrophages in these organs.⁴⁰ A recent report showed that nanomaterials could be cleared from the liver and spleen within 7 days after injection, thereby ensuring their biosafety.⁴¹ The tissues contain high background levels of iron, and therefore, much higher iron than Gd and Mn was detected in the tissues. Furthermore, the concentration of iron in the spleen is higher than that in the liver after exposure to 3 nm sized ESIONs. It should be noted that Gd levels observed in the kidneys of the GDI-treated group were

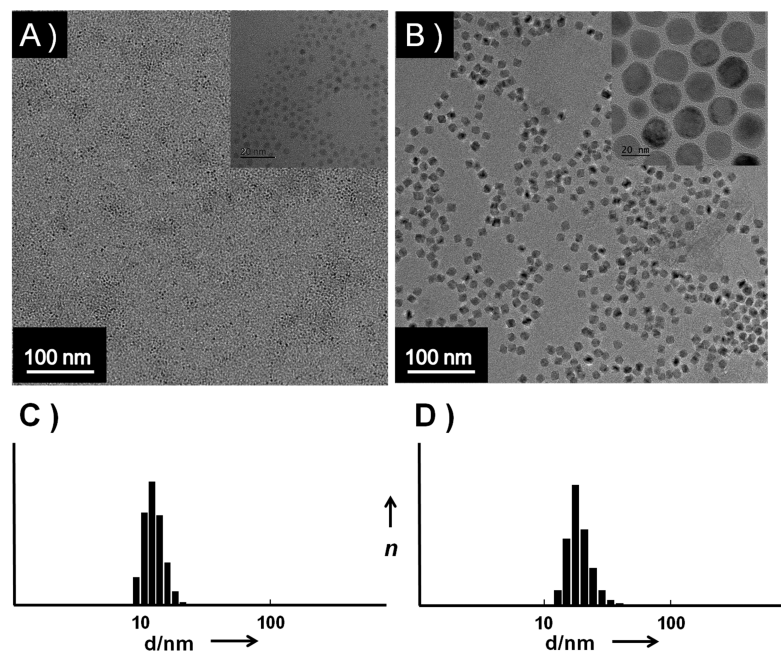


Figure 1. Transmission electron microscopy (TEM) images of (A) extremely small-sized iron oxide nanoparticles (ESIONs), and (B) manganese oxide nanoparticle (MnO NPs). In the inset of (A) and (B), high magnification TEM images are shown, and the scale bar is 20 nm. Dynamic Light Scattering (DLS) size measurement of (C) ESIONs and (D) MnO NPs.

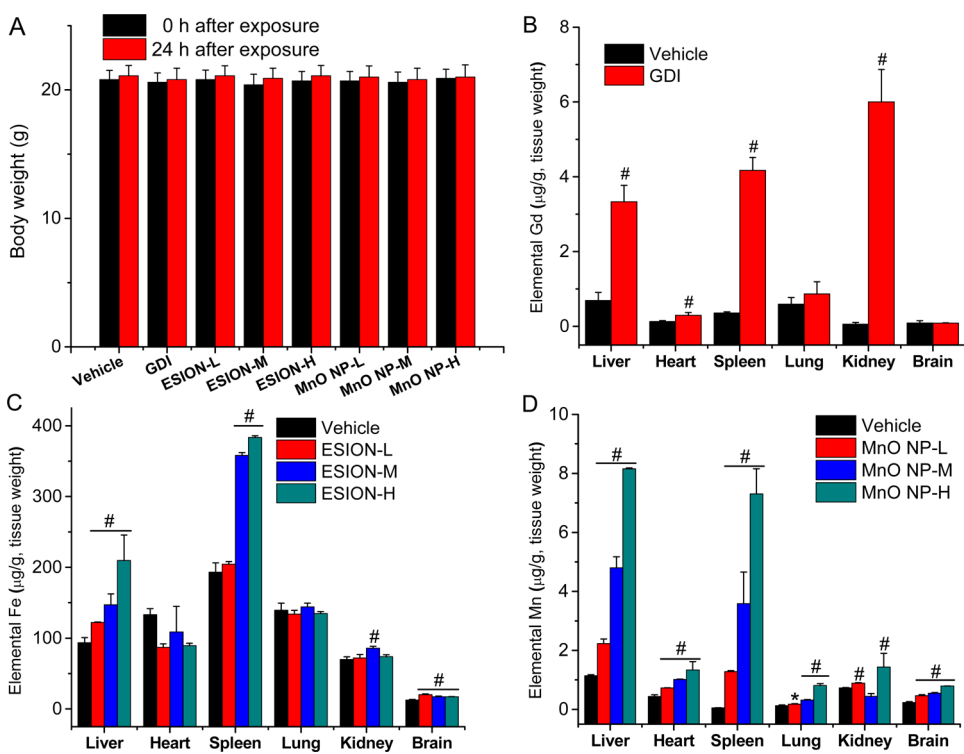


Figure 2. Body weight results and inductively coupled plasma-mass spectrometry (ICP-MS) analysis of Gd, Fe, and Mn elements in various organ and tissues after 24-h exposure. (A) body weights of mice after tail intravenous injection; (B) GDI, 0.2 μ mol/g body weight; (C) ESIONs; (D) MnO NPs. L, low-dose group, 2 μ g/g; M, medium-dose group, 5 μ g/g; and H, high-dose group, 10 μ g/g. Data are mean \pm SD, $n = 3$; * $P < 0.05$, # $P < 0.001$ compared with vehicle control group. GDI, gadopentetate dimeglumine injection; ESIONs, extremely small-sized iron oxide NPs; MnO NPs, manganese oxide nanoparticles.

significantly higher than those in the kidneys of the other groups (Figure 2B). A similar accumulation of elemental Gd in the kidneys following GBCA exposure has been reported in rodents and primate.^{42–45}

Comparatively, while iron was not accumulated in the kidney tissues, Mn showed a significantly higher accumulation in the high-dose group than it did in the low-dose. These results suggest that elemental Gd has a

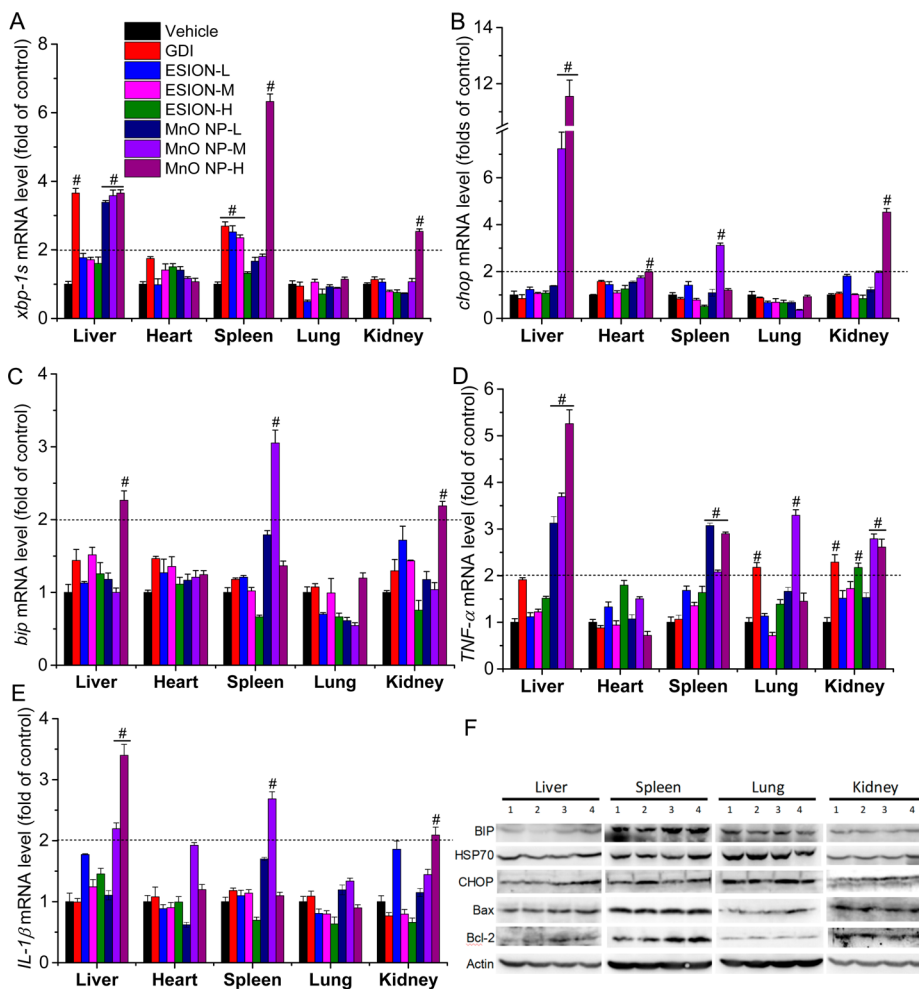


Figure 3. Changes in marker gene and proteins after 24-h exposure to contrast agents. Representative RT-PCR results from three repeated tests: (A) *xbp-1s*, (B) *chop*, (C) *bip*, (D) *TNF- α* , and (E) *IL-1 β* . Dotted type lines indicate genes differentially expressed with >2 -fold change. $^{\#}P < 0.001$ indicates statistically significant comparing to the vehicle control group when folds of the expression value higher than 2. (F) Expression levels of AOP marker proteins after 24-h treatment of mice with contrast agents at high-dose (0.2 μ mol/g for GDI, 10 μ g/g for ESION, and MnO NPs). No. 1, Vehicle control; 2, GDI; 3, ESIONs; 4, MnO NPs. *Chop*, CCAAT-enhancer-binding protein homologous protein gene; *bip*, binding immunoglobulin protein gene; *TNF- α* , tumor necrosis factor- α gene; *IL-1 β* , interleukin-1 β gene; AOP, adverse outcome pathway; GDI, gadopentetate dimeglumine; ESIONs, extremely small-sized iron oxide NPs; MnO NPs, manganese oxide nanoparticles.

high property to be accumulated in the kidneys.⁴² The GBCA accumulation in the kidney lasting for at least 24 h increases the chances of exposure to Gd ion, thereby increasing the likelihood of toxic potential.⁷ The corresponding elements were also found by ICP-MS in heart, lung, and brain (Figure 2B–D). However, the absolute mass concentration of these measurements may be overestimated due to the contributions from the blood residue in these tissues.

The protein corona may be formed after PEG modified NPs entering in the blood. It is generally accepted that the protein corona serves to equalize the surface charge of NPs and increase the biocompatibility.^{46,47} The serum proteins in the corona inhibit the cellular uptake of NPs by increasing corona surface free energy for decreased contact of NPs with cell membrane.⁴⁸ It was found that this inhibitory effect is more prominent for NPs in phagocytic cells than for

those in nonphagocytic cells.⁴⁸ Another *in vitro* study shows that the protein corona is strong enough to be retained on the NPs as they enter cells *via* endocytosis, and then the corona are degraded inside cell lysosome.⁴⁹ Further, it is interesting that the small sized (<20 nm) NPs usually have lower cellular uptake level than larger sized (>50 nm) ones, although corona of larger NPs have a higher inhibition ability to cellular uptake than small ones.⁴⁸ These studies indicate that small sized NPs may have some advantages for biomedical imaging including MRI applications due to their long time retention in blood circulation. In the current study, the corona forming ability and particle aggression level were relatively low based on the *in vitro* stability test of our NPs in serum contained medium (Figure S1).

Effects on the Expression Levels of AOP Markers. No acute toxicity was observed after exposure to the contrast

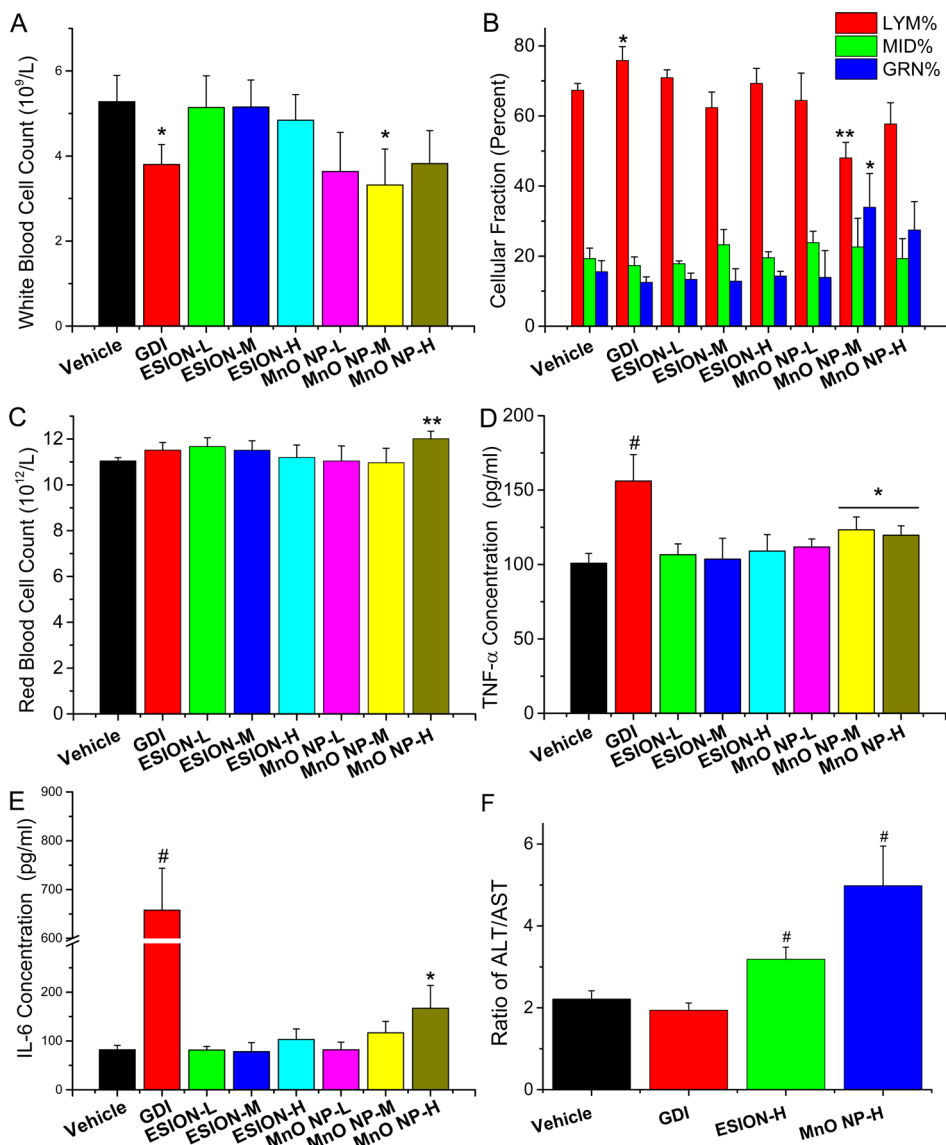


Figure 4. Hematological changes and inflammation levels after 24-h exposure to contrast agents. (A) total white blood cell (WBC) count; (B) percentages of lymphocytes (LYM), precursor white cells (MID, minimum inhibitory dilution), and granulocytes (GRN) in total cell counts; (C) total red blood cell (RBC) count; (D) tumor necrosis factor (TNF)- α , and (E) interleukin (IL)-6 production levels in serum. (F) liver function test. Ratio of alanine transaminase (ALT) to aspartate transaminase (AST) represents liver damages caused from intravenous exposure to contrast agents. Data are mean \pm SD, $n = 3$; * $P < 0.05$, ** $P < 0.01$, and # $P < 0.001$ compared with vehicle control group.

agents at MRI clinical application doses. Therefore, the sensitive reverse transcription-polymerase chain reaction (RT-PCR) was used to detect alterations in gene transcription levels depicting interruption of the AOP. Figure 3 illustrates the effects of contrast agent-induced ER stress responses and inflammations on various tissues. After exposure for 24 h, the specific marker gene *xbp-1* splicing (*xbp-1s*) was significantly upregulated in the spleen and liver of the GDI and MnO NP groups but only in the spleen of the ESION group. The CCAAT-enhancer-binding protein homologous protein (*chop*) gene was induced in the liver, spleen, and kidney in the MnO NP-treated groups, but not the GDI and ESION NP-treated groups (Figure 3B). The upregulation of this gene led to the overexpression

of CHOP protein in the liver after exposure to high-dose MnO NPs as indicated in the Western blot results (Figure 3F). The *xbp-1s* is a typical marker of the ER stress response and it initiates a series of molecular events required for the induction of the self-protection mechanism.⁵⁰ CHOP (also known as DNA-damage-inducible transcript 3, DDIT3) has been found to be involved in ER stress-related apoptosis, which is caused by unsuccessful self-recovery after the activation of the ER stress pathway.⁵¹ Therefore, the overexpression of these two genes could be used as early and sequential biomarkers in safety evaluations.^{28,29} Furthermore, the changes in the binding immunoglobulin protein (*bip*) gene and protein exhibited a similar trend shown by *chop* in various tissues (Figure 3C,F). The MnO NPs

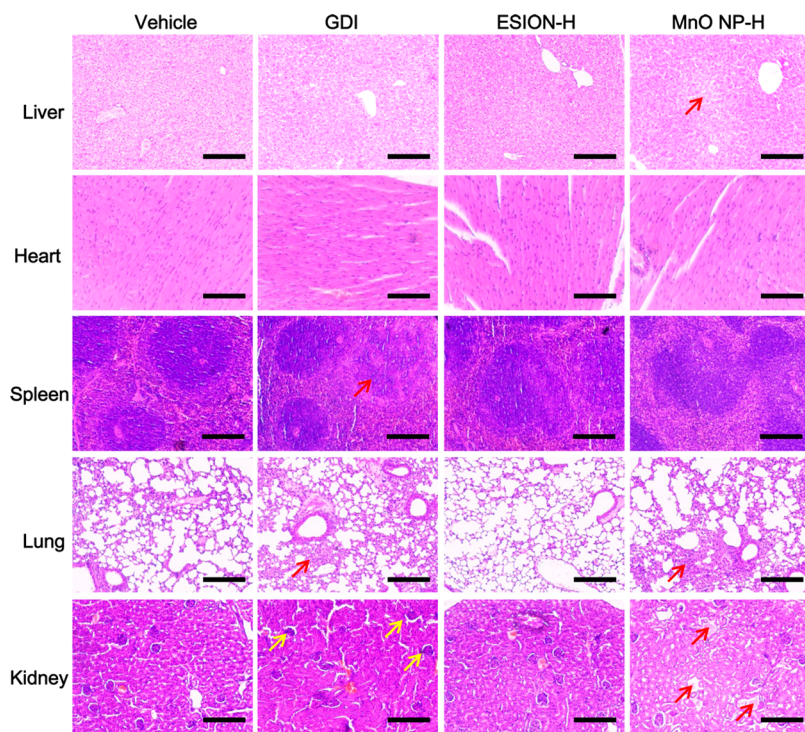


Figure 5. Histopathological images of mouse tissue after 24-h intravenous exposure to contrast agents. Red arrows show obvious pathological changes in cells including swelling/atrophy; yellow arrows show significantly widened renal capsule. Scale bar = 200 μ m.

induced a high inflammatory response that was associated with the upregulation of tumor necrosis factor- α (*TNF- α*) and interleukin-1 β (*IL-1 β*) genes. Comparatively, GDI exposure induced significant overexpression of *TNF- α* in the lung and kidney, while ESION treatment produced similar overexpression in the kidney of the high-dose group, but no obvious changes were observed in the expression of the *IL-1 β* gene (Figure 3D,E). Our results collaborate well with other reports regarding iron oxide NPs' safe characters in cell tracking applications. For example, the gene expression profiling had shown that no obvious adverse effects on cell viability, function, and gene expression after cells labeled with iron oxide NPs by endocytosis.⁵² MRI cell tracking is an important application for iron oxide nanoparticles in clinical diagnosis.⁵³ Different to the direct usage as T1 contrast agents, iron oxide NP should be first endocytosed into cells before injection of the labeled cells for MRI cell tracking research; consequently, the NP is usually designed to be positively charged for *in vitro* cellular uptake, while to be neutral or negatively charged for *in vivo* blood circulations for conventional MRI diagnostic application, *i.e.*, ESIONs in this research.⁵³ It is supposed that the acidic condition of lysosome can trigger Fe^{3+} released from intercellular iron oxide NPs, then affecting normal cellular functions by interruption the iron homeostasis.⁵³ One *in vitro* test report showed that iron oxide NPs activated the cellular signaling responsible for cell migration and hence inhibit osteogenesis in human

mesenchymal stem cell at a quite high concentration (300 μ g/mL).⁵⁴ PEG coated iron oxide NPs show much lower toxicities than their bare counterparts,^{55,56} which illustrates the high safety of the MRI application of our ESIONs.

Hematological Analysis. The total white blood cell (WBC) count was unaffected in exposure to ESIONs for 24 h. However, there were significant decreases in the total WBC of the GDI- and medium-dose MnO NP-treated groups (Figure 4A). The GDI- and the same medium-dose MnO-treated groups showed a higher percentage of lymphocytes and granulocytes, respectively and these differences in the affected cells suggest that these contrast agents may have different toxicity mechanisms (Figure 4B). The hematology data showed a significant increase in red blood cells (RBC) in the high-dose MnO NP-treated group (Figure 4C). Significant increases in *TNF- α* and *IL-6* were observed in the serum of the GDI-treated group (Figure 4D,E). These results are in agreement with previous reports linking inflammation to the release of Gd ions from GBCAs and may be the mechanism to underlie the development of nephrogenic systemic fibrosis (NSF).^{33,34} In addition, the liver function in high dose ESION and MnO NP treatment groups was significantly decreased as shown by the increase in the alanine transaminase (ALT) to aspartate transaminase (AST) ratio, which is an obvious marker of hepatocellular injury (Figure 4F). This result suggests nanoparticles may have higher influencing results to liver than GDI in the earlier 24 h.

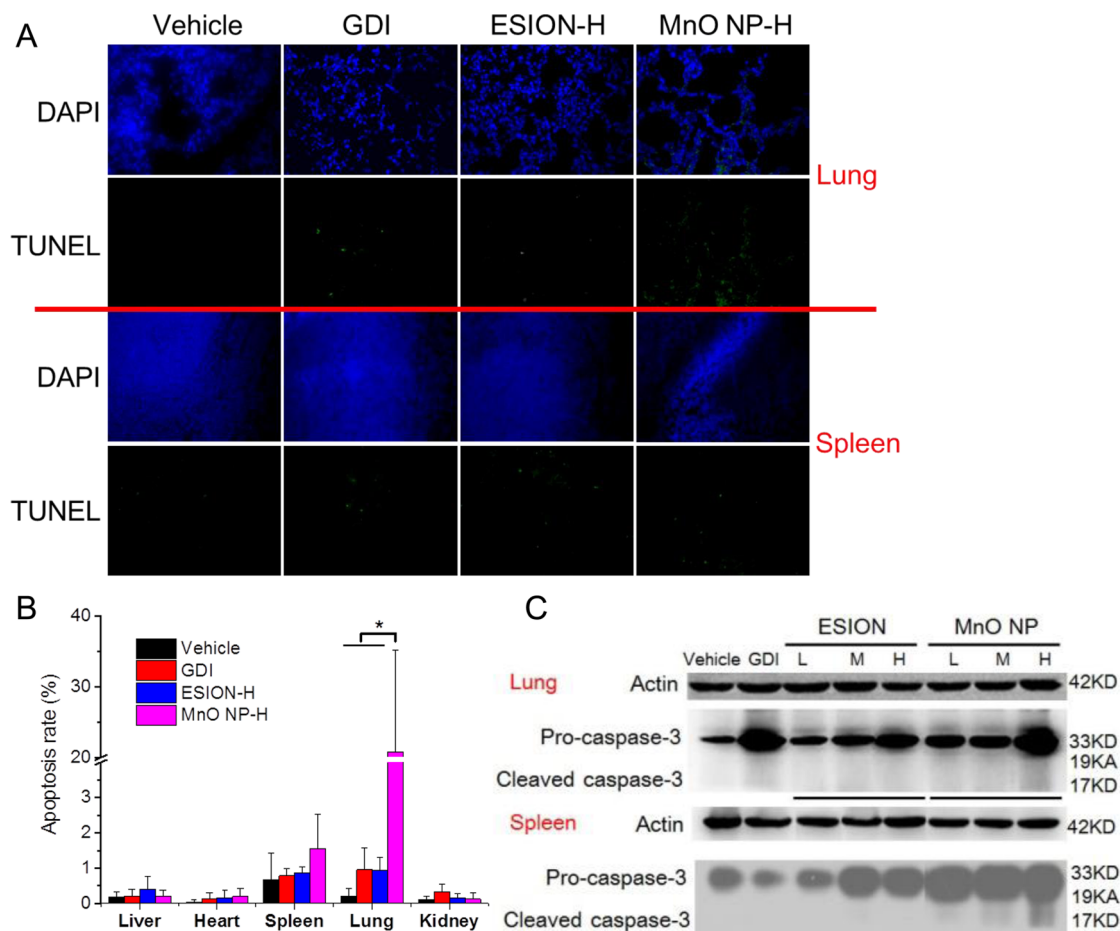


Figure 6. Apoptosis results of mouse tissues after 24-h intravenous exposure to contrast agents. (A) representative images of mouse lung and spleen tissue in terminal deoxynucleotidyl transferase dUTP nick end labeling (TUNEL) assay after intravenous exposures to contrast agents for 24 h. Cells with bright fluorescence were counted as TUNEL positive cells. (B) apoptosis rate of TUNEL assay after intravenous exposure to contrast agents for 24 h in mice. Results are expressed as mean \pm SD, * P < 0.001 compared to indicated groups of same tissue. (C) Western blot of Caspase-3 protein in lung and spleen tissue after treatment with contrast agents at indicated doses. L, low-dose group, 2 μ g/g; M, medium-dose group, 5 μ g/g; H, high-dose group, 10 μ g/g.

Histopathological Effects of High-Dose Contrast Agents. A histopathological examination of mouse tissue from high-dose GDI- and contrast agent-treated groups was performed.⁵⁷ The MnO NPs induced significant pathological changes in the liver, lungs, and kidneys of treated mice (Figure 5). There were obvious changes in the liver tissue including disorganized hepatic cords, damaged hepatic lobules, and mild vacuolar degeneration. In the spleen, the lymphocyte number significantly decreased in the lymphoid nodules accompanied by the disappearance of the germinal center following GDI exposure. Both GDI and MnO NP treatments induced obvious damage to the lungs and kidneys. Slightly thickened alveolar walls as well as multifocal consolidation and infiltration of focal inflammatory cells occurred in the lung, while atrophy of the glomerular and renal tubular epithelial cells, shortened tube cavity, and slightly transparent tube types were found in the kidneys. However, exposure to high-dose ESION did not induce any observable impairment to the evaluated tissues.

Apoptosis Analysis. Apoptosis was evaluated using the fluorescence-conjugated terminal deoxynucleotidyl transferase dUTP nick end labeling (TUNEL) assay (Figure 6A). The level of apoptotic cells in the lungs of the high-dose MnO NP-exposed group is significantly higher than that found in the vehicle control, GDI-, and ESION-treated groups (Figure 6B). Similar results were observed with the level of Bcl-2-associated X (Bax) protein in the lung tissue of the high-dose-treated groups (Figure 3F). Exposure to GDI and ESIONs did not induce acute apoptosis. Caspases are executors of cellular apoptosis in signaling events after stimulation and the Western blot analysis of caspase-3 levels in the lung and spleen correlated with the TUNEL detection results (Figure 6C). Furthermore, MnO NPs showed a higher apoptosis-inducing ability than GDI and iron oxide NPs did, and there was no significant difference between the GDI or ESION treatments. Therefore, the apoptosis analysis suggests that GDI and ESIONs may both possess a good safety profile at MRI application doses. However, the safety evaluation of contrast

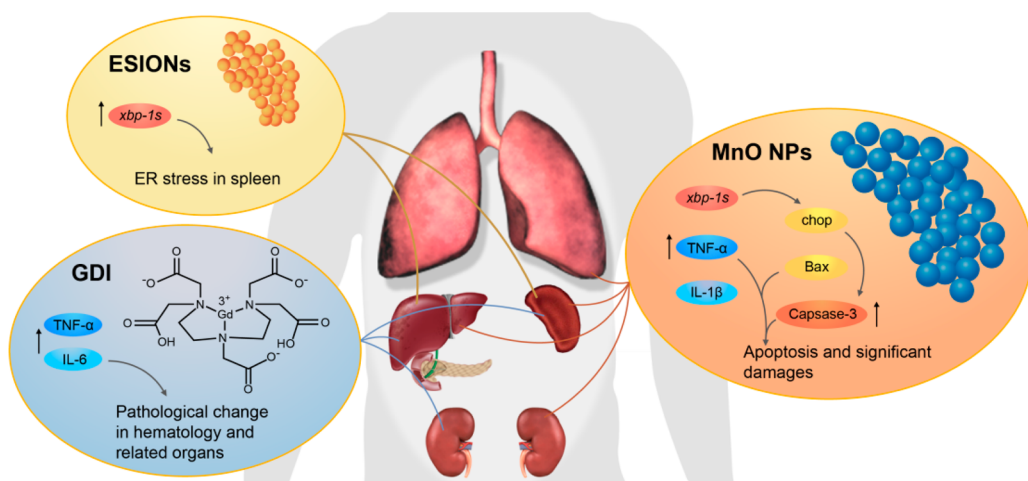


Figure 7. Schematic illustration of biodistributions and related toxic responses after *in vivo* exposure to contrast agents in magnetic resonance imaging (MRI) scanning process.

agents should consider various other adverse effects involving different physiological processes (Figure 7).⁵⁸ Furthermore, damage and inflammation were observed in the tissues of MnO NP- and GDI-treated groups, but only ER stress was evident in the spleen of ESION-treated mice after exposure for 24 h.

There are many coating materials for NPs. It is much more complex after binding with different proteins on the coated material surfaces of NPs. For iron oxide NPs, different characteristics lead to various cell responses by forming various protein coronas. Some proteins, *i.e.*, albumin, are easily adsorbed on positively charged coatings, but others, *i.e.*, fibrinogen, only binding on negatively charged iron oxide NPs.⁵⁹ The binding of protein corona generally leads to equalization of the surface charge of the coating of NPs after the electrostatic adsorption. Negatively charged SPIONs showed the most biocompatible than positively charged or naked ones by the toxicity end point of cellular proliferation reduction.⁵⁹ The decrease in toxicity from coating is thought to arise from blocking the ROS generation from iron oxide NPs.⁶⁰ Thus far, PEGylation is one of the most widely used approaches to enhance the colloidal stability of iron oxide NPs in serum-rich biological environment, and the PEGylated NPs exhibit much lower cellular uptake than NPs coated by small molecular ligands or polyelectrolytes.⁶¹ For GDI, gadolinium ions dissociated from the matrix mainly contribute to the toxic effect; While the basic toxic mechanism for NPs are thought to come from the high surface area and surface ion leaching. In this study, although PEGylation was used to increase the blood half-lives of NPs, the enrollment of NPs in the tissue cells is inevitable. 3-nm-sized ESIONs or 15 nm-sized MnO particles mean highly reactive surface, and once enrolled in the tissue cell, they can initiate the intracellular toxicity through the generation of ROS which damage the contacted biological molecules. It is well accepted that the acidic environment of

cellular lysosomes can trigger the dissolution of NP surface ions, which also mediate ROS generation. Further, the toxicity of Mn ion had been observed and well summarized previously.^{62–64} Its toxicity lies on the valence state of Mn and the disturbance outcome on the homeostasis of pro-oxidant and anti-oxidant factors, which leads to the toxic damages, *i.e.*, oxidation of biological molecules. These adverse effects can cause stress and nonreversible genetic mutations by interfering with the signaling pathway directly or indirectly. In summary, our results demonstrate that ESIONs are quite safe when used as contrast agents, and provide critical information on their novel function in clinical MRI applications.

CONCLUSION

The purpose of this study was to evaluate the biosafety of different contrast agents in order to provide their potential clinical benefits. Therefore, the *in vivo* biosafety of novel oxide NP-based T1 MRI contrast agents, ESION and MnO NPs, and the clinically used gadolinium-based contrast agent was compared using a mouse model. From our results, ESIONs showed a better safety profile and more favorable properties than MnO NPs and GBCAs. In summary, our findings revealed that at the simulated clinical doses for MRI applications, ESIONs exhibit a considerably more stable safety profile. This novel contrast agent may be more suitable for future clinical applications than the MnO-based T1 contrast agent and the clinically used GDI GBCA. Furthermore, GDI induced a high accumulation of gadolinium in the liver, spleen, and especially kidneys. This organ-specific accumulation induced by GDI indicates a high potential risk of developing chronic diseases (*e.g.*, NSF) associated with long-term exposure to gadolinium ion. The ESIONs with mean size of 3 nm were mostly concentrated in the spleen and, therefore, induced only stress related effects and no other severe damage. Therefore, we propose that

ESIONs mainly composed of iron have a great potential to serve as a promising contrast agent in the future clinical MRI applications. Our results suggest that the

development of well-characterized nanomaterials is an exciting prospect for the improvement of the health safety and clinical therapeutic benefits of contrast MRI.

MATERIALS AND METHODS

Materials. GDI was provided by the Beijing Haidian Hospital Medical Imaging Department (Beijing, China). ESIONs and MnO NPs were prepared according to the previously reported methods.^{13,14} They were diluted in sterile Milli-Q water to prepare stock solutions (1 mg/mL), which were sonicated in an ultrasound bath (100 W) for 5 min and diluted with Milli-Q water for TEM analysis using the JEM-200CX transmission electron microscope (JEOL, Japan). The hydrodynamic diameter and zeta-potential of NPs were measured by a Malvern Zeta sizer Nano ZS instrument (Malvern Instruments, U.K.) after dilution in corresponding dilutions. The primary antibodies including anti-caspase-3 and anti-actin were purchased from Santa Cruz Biotechnology (Santa Cruz, CA), and the TUNEL assay kit was purchased from Roche Life Science (Indianapolis, IN).

Animal Exposure. Balb/c mice (20–22 g) were provided by the Beijing Vital River Experimental Animal Technology Co. Ltd., and housed in an isolated animal room with water and rodent food supplements. The animals were acclimated to the environment for 1 week prior to the experiments. All procedures were approved by the Ethics Committee of the Animal Care and Experimentation of the National Institute for Environmental Studies, China. The mice were randomly divided into seven groups ($n = 6$): a vehicle control (saline), 0.2 μ mol/g GDI-treated, and 2, 5, 10 μ g/g bw ESION or MnO NP-treated groups. The tail vein intravenous injection was used for the contrast agent exposure. Then, the body weights of mice from all groups were recorded. After 24 h, animals were weighted again and euthanized for toxic responses analysis. At necropsy, the animals were anesthetized with 40 mg/kg intraperitoneal sodium pentobarbital and blood samples were collected by the standard operation procedures for a routine animal blood draw. Furthermore, tissues and organs such as the heart, liver, spleen, kidneys, and lung were excised and accurately weighed.

Hematological and Biochemical Analyses. About 1 mL of blood was drawn by removing the eyeball of the mice before necropsy. Then, 100 μ L of whole blood was directly placed in tubes containing ethylenediaminetetraacetic acid (EDTA) for hematological analysis (Deyuan Co., Beijing, China). In addition, about 900 μ L of blood was allowed to clot for the serum separation and biochemical analysis. IL-6 and TNF- α levels were analyzed using a mouse IL-6/TNF- α specific enzyme-linked immunosorbent assay (ELISA) kit (eBioscience, San Diego, CA), following the manufacturer's instructions. Results were expressed in picograms per milliliter (pg/mL), and three independent experiments were performed.

ICP-MS. Elemental Gd, Fe, and Mn in the GDI-, ESION-, and MnO NP-exposed groups, respectively, were separately quantified using ICP-MS. Briefly, samples (about 100 mg) were pre-digested overnight with 5.0 mL of concentrated nitric acid (HNO_3 , MOS grade), mixed with 1.0 mL of 30% hydrogen peroxide (H_2O_2 , MOS grade), and then digested for 2 h in open vessels on a hot plate at 150 °C. Finally, the remaining solution (about 0.5 mL) was cooled and diluted to 3.0 mL with 2% HNO_3 . Indium (In) was used as the internal standard throughout the test. Both standard and test solutions were measured thrice using ICP-MS (PerkinElmer, Waltham, MA).

RT-PCR, Quantitative Real-Time (q) PCR, and Western Blot Analysis. The procedures used for the RT-PCR, quantitative real-time (q) PCR, and Western blot analysis were the same as previously described.²⁹ Briefly, the total RNA was isolated from mouse livers and spleens with TRIzol (Invitrogen) extraction. After quantification of the extracted RNA pellets, first-strand complementary DNA synthesis was performed using a Superscript First-Strand Synthesis kit (Invitrogen). All samples were analyzed by qPCR (Eppendorf, Germany) using the SYBR Green PCR

Master Mix with reaction in volumes of 25 μ L. The primers used are listed in Table S1. Protein samples were obtained by homogenizing the frozen tissues in a lysis buffer containing 20 mM Tris-HCl, 150 mM sodium chloride (NaCl), 1 mM EDTA, 1 mM ethylene glycol tetraacetic acid (EGTA), 1% Triton-X 100, and a protease inhibitor (pH 7.4) followed by centrifugation for 15 min at 10 000 \times g and the tissue debris obtained at 4 °C was discarded. The supernatants were collected, and the protein concentrations were determined using a Bio-Rad kit. The proteins were separated on sodium dodecyl sulfate-polyacrylamide (SDS-PAGE) gels, transferred to nitrocellulose membranes, and then incubated with the desired antibodies, which were purchased from Santa Cruz Biotechnology (Santa Cruz, CA). The blot signals were developed using horseradish peroxidase (HRP)-conjugated secondary antibodies and enhanced chemiluminescence (ECL) solution (Thermo Scientific).

TUNEL Assay. The TUNEL assay was used to specifically detect the fragmented genomic DNA usually caused by sequential activation of caspases and endonucleases during apoptosis. Dewaxing, tissue rehydration, and staining were carried out according to the recommended procedures of the fluorescence-conjugated TUNEL kit manufacturer (Roche, Mannheim, Germany). For counting the total number of cells in tissue samples, DAPI was added before mounting the coverslips to stain the nuclei. Images were captured with a fluorescence microscope (Olympus BX61WI with Fluoview FV1000 software, Japan), and then analyzed using the ImagePro software. Three different image areas of at least 500 cells were counted to determine the apoptosis rate.

Histopathological Examination. The histopathological analysis was performed following standard procedures.⁶⁵ Briefly, the organ tissues were fixed overnight in 10% neutral-buffered formalin, embedded in paraffin blocks, cut into 4- μ m sections, and mounted onto glass slides. After hematoxylin and eosin (H&E) staining, the pathological changes in the tissues were observed under an optical microscope (Leica DM4000M, Germany) by a well-trained pathologist.

Statistics. The data were presented as mean \pm standard deviation (SD). The statistical analyses were performed using Student's *t*-test for comparison of two paired groups and *P*-values < 0.05 were considered statistically significant.

Conflict of Interest: The authors declare no competing financial interest.

Supporting Information Available: The Supporting Information is available free of charge on the ACS Publications website at DOI: 10.1021/acsnano.5b05783.

Additional figures and table, including figure of GBCA chemical formula and PCR primer information table (PDF)

Acknowledgment. T.H. acknowledges financial support by the Research Center Program of the Institute for Basic Science (IBS) in Korea (IBS-R006-D1); D.L. acknowledges the National Natural Science Foundation of China (51503180), "Thousand Talents Program" for Distinguished Young Scholars (588020*G81501/048) and Fundamental Research Funds for the Central Universities (520002*172210151); R.C., C.C., and Y.Z. acknowledge financial support by the Ministry of Science and Technology of China (2011CB933401 and 2012CB934003), the National Natural Science Foundation of China (21477029, 21320102003, 21277037, 21277080), the Chinese Academy of Sciences (XDA09040400), Major Project of the National Social Science Fund (Grant No. 12&ZD117) "Ethical issues of high-tech," Beijing Key Laboratory of Environmental Toxicology (2015HJDL01) and the National Science Fund for Distinguished Young Scholars (11425520).

REFERENCES AND NOTES

- Lartigue, L.; Hugounenq, P.; Alloyeau, D.; Clarke, S. P.; Levy, M.; Bacri, J. C.; Bazzi, R.; Brougham, D. F.; Wilhelm, C.; Gazeau, F. Cooperative Organization in Iron Oxide Multi-Core Nanoparticles Potentiates Their Efficiency as Heating Mediators and MRI Contrast Agents. *ACS Nano* **2012**, *6*, 10935–10949.
- Floyd, W. C.; Klemm, P. J.; Smiles, D. E.; Kohlgruber, A. C.; Pierre, V. C.; Mynar, J. L.; Frechet, J. M.; Raymond, K. N. Conjugation Effects of Various Linkers on Gd(III) MRI Contrast Agents with Dendrimers: Optimizing the Hydroxypyridinone (HOPO) Ligands with Nontoxic, Degradable Esteramide (EA) Dendrimers for High Relaxivity. *J. Am. Chem. Soc.* **2011**, *133*, 2390–2393.
- Runge, V. M. Magnetic Resonance Imaging Contrast Agents. *Curr. Opin. Radiol.* **1992**, *4*, 3–12.
- De Haen, C. Conception of the First Magnetic Resonance Imaging Contrast Agents: a Brief History. *Top. Magn. Reson. Imaging* **2001**, *12*, 221–230.
- Weinmann, H. J.; Brasch, R. C.; Press, W. R.; Wesbey, G. E. Characteristics of Gadolinium-DTPA Complex: a Potential NMR Contrast Agent. *AJR, Am. J. Roentgenol.* **1984**, *142*, 619–624.
- Rose, T. A.; Choi, J. W. Intravenous Imaging Contrast Media Complications: the Basics That Every Clinician Needs to Know. *Am. J. Med.* **2015**, *128*, 943–949.
- Chopra, T.; Kandukurti, K.; Shah, S.; Ahmed, R.; Panesar, M. Understanding Nephrogenic Systemic Fibrosis. *Int. J. Nephrol.* **2012**, *2012*, 912189.
- Penfield, J. G.; Reilly, R. F. What Nephrologists Need to Know About Gadolinium. *Nat. Clin. Pract. Nephrol.* **2007**, *3*, 654–668.
- Ling, D.; Hyeon, T. Chemical Design of Biocompatible Iron Oxide Nanoparticles for Medical Applications. *Small* **2013**, *9*, 1450–1466.
- Na, H. B.; Song, I. C.; Hyeon, T. Inorganic Nanoparticles for MRI Contrast Agents. *Adv. Mater.* **2009**, *21*, 2133–2148.
- Elsabahy, M.; Heo, G. S.; Lim, S. M.; Sun, G.; Wooley, K. L. Polymeric Nanostructures for Imaging and Therapy. *Chem. Rev.* **2015**, *115*, 10967–11011.
- Ling, D.; Lee, N.; Hyeon, T. Chemical Synthesis and Assembly of Uniformly Sized Iron Oxide Nanoparticles for Medical Applications. *Acc. Chem. Res.* **2015**, *48*, 1276–1285.
- Kim, B. H.; Lee, N.; Kim, H.; An, K.; Park, Y. I.; Choi, Y.; Shin, K.; Lee, Y.; Kwon, S. G.; Na, H. B.; et al. Large-Scale Synthesis of Uniform and Extremely Small-Sized Iron Oxide Nanoparticles for High-Resolution T1 Magnetic Resonance Imaging Contrast Agents. *J. Am. Chem. Soc.* **2011**, *133*, 12624–12631.
- Na, H. B.; Lee, J. H.; An, K.; Park, Y. I.; Park, M.; Lee, I. S.; Nam, D. H.; Kim, S. T.; Kim, S. H.; Kim, S. W.; et al. Development of a T1 Contrast Agent for Magnetic Resonance Imaging Using MnO Nanoparticles. *Angew. Chem., Int. Ed.* **2007**, *46*, 5397–5401.
- Pösel, E.; Kloust, H.; Tromsdorf, U.; Janschel, M.; Hahn, C.; Maßlo, C.; Weller, H. Relaxivity Optimization of a PEGylated Iron-Oxide-Based Negative Magnetic Resonance Contrast Agent for T 2-Weighted Spin-Echo Imaging. *ACS Nano* **2012**, *6*, 1619–1624.
- Lee, N.; Hyeon, T. Designed Synthesis of Uniformly Sized Iron Oxide Nanoparticles for Efficient Magnetic Resonance Imaging Contrast Agents. *Chem. Soc. Rev.* **2012**, *41*, 2575–2589.
- Pernia Leal, M.; Rivera-Fernandez, S.; Franco, J. M.; Pozo, D.; De la Fuente, J. M.; Garcia-Martin, M. L. Long-Circulating Pegylated Manganese Ferrite Nanoparticles for MRI-Based Molecular Imaging. *Nanoscale* **2015**, *7*, 2050–2059.
- Im, G. H.; Kim, S. M.; Lee, D.-G.; Lee, W. J.; Lee, J. H.; Lee, I. S. $\text{Fe}_3\text{O}_4/\text{MnO}$ Hybrid Nanocrystals as a Dual Contrast Agent for Both T 1-and T 2-Weighted Liver MRI. *Biomaterials* **2013**, *34*, 2069–2076.
- Zhou, J.; Sun, Y.; Du, X.; Xiong, L.; Hu, H.; Li, F. Dual-Modality *in Vivo* Imaging Using Rare-Earth Nanocrystals with Near-Infrared to Near-Infrared (NIR-To-NIR) Upconversion Luminescence and Magnetic Resonance Properties. *Biomaterials* **2010**, *31*, 3287–3295.
- Liu, Y.; Yang, K.; Cheng, L.; Zhu, J.; Ma, X.; Xu, H.; Li, Y.; Guo, L.; Gu, H.; Liu, Z. PEGylated $\text{FePt}@\text{Fe}_2\text{O}_3$ Core-Shell Magnetic Nanoparticles: Potential Theranostic Applications and *in Vivo* Toxicity Studies. *Nanomedicine* **2013**, *9*, 1077–1088.
- Cheng, L.; Yang, K.; Li, Y.; Zeng, X.; Shao, M.; Lee, S.-T.; Liu, Z. Multifunctional Nanoparticles for Upconversion Luminescence/MR Multimodal Imaging and Magnetically Targeted Photothermal Therapy. *Biomaterials* **2012**, *33*, 2215–2222.
- Xiao, J.; Tian, X. M.; Yang, C.; Liu, P.; Luo, N. Q.; Liang, Y.; Li, H. B.; Chen, D. H.; Wang, C. X.; Li, L.; et al. Ultrahigh Relaxivity and Safe Probes of Manganese Oxide Nanoparticles for *in Vivo* Imaging. *Sci. Rep.* **2013**, *3*, 3424.
- Luo, K.; Liu, G.; He, B.; Wu, Y.; Gong, Q.; Song, B.; Ai, H.; Gu, Z. Multifunctional Gadolinium-Based Dendritic Macromolecules as Liver Targeting Imaging Probes. *Biomaterials* **2011**, *32*, 2575–2585.
- Zhen, L.; Li, Z.; Liu, J.; Song, G.; Yuan, Q.; Ren, J.; Qu, X. Long-Circulating Er^{3+} -Doped Yb_2O_3 Up-Conversion Nanoparticle as an *in Vivo* X-Ray CT Imaging Contrast Agent. *Biomaterials* **2012**, *33*, 6748–6757.
- Tian, X.; Guan, X.; Luo, N.; Yang, F.; Chen, D.; Peng, Y.; Zhu, J.; He, F.; Li, L.; Chen, X. *In Vivo* Immunotoxicity Evaluation of Gd_2O_3 Nanoprobes Prepared by Laser Ablation in Liquid for MRI Preclinical Applications. *J. Nanopart. Res.* **2014**, *16*, 2594.
- Firestone, M.; Kavlock, R.; Zenick, H.; Kramer, M. The US Environmental Protection Agency Strategic Plan for Evaluating the Toxicity of Chemicals. *J. Toxicol. Environ. Health, Part B* **2010**, *13*, 139–162.
- Krewski, D.; A. D., Jr.; Andersen, M.; Anderson, H.; Boekelheide, K.; Brent, R.; Charnley, G.; Cheung, V. G.; G, S., Jr. Toxicity Testing in the 21st Century: a Vision and a Strategy. *J. Toxicol. Env. Health, B* **2010**, *13*, 51–138.
- Huo, L.; Chen, R.; Zhao, L.; Shi, X.; Bai, R.; Long, D.; Chen, F.; Zhao, Y.; Chang, Y.-Z.; Chen, C. Silver Nanoparticles Activate Endoplasmic Reticulum Stress Signaling Pathway in Cell and Mouse Models: the Role in Toxicity Evaluation. *Biomaterials* **2015**, *61*, 307–315.
- Chen, R.; Huo, L.; Shi, X.; Bai, R.; Zhang, Z.; Zhao, Y.; Chang, Y.; Chen, C. Endoplasmic Reticulum Stress Induced by Zinc Oxide Nanoparticles Is an Earlier Biomarker for Nanotoxicological Evaluation. *ACS Nano* **2014**, *8*, 2562–2574.
- Yoshida, H.; Matsui, T.; Yamamoto, A.; Okada, T.; Mori, K. XBP1 mRNA Is Induced by ATF6 and Spliced by IRE1 in Response to ER Stress to Produce a Highly Active Transcription Factor. *Cell* **2001**, *107*, 881–891.
- Lin, J. H.; Li, H.; Yasumura, D.; Cohen, H. R.; Zhang, C.; Panning, B.; Shokat, K. M.; Lavail, M. M.; Walter, P. IRE1 Signaling Affects Cell Fate During the Unfolded Protein Response. *Science* **2007**, *318*, 944–949.
- Nakagawa, T.; Zhu, H.; Morishima, N.; Li, E.; Xu, J.; Yankner, B. A.; Yuan, J. Caspase-12 Mediates Endoplasmic-Reticulum-Specific Apoptosis and Cytotoxicity by Amyloid-Beta. *Nature* **2000**, *403*, 98–103.
- Xia, Q.; Feng, X.; Huang, H.; Du, L.; Yang, X.; Wang, K. Gadolinium-Induced Oxidative Stress Triggers Endoplasmic Reticulum Stress in Rat Cortical Neurons. *J. Neurochem.* **2011**, *117*, 38–47.
- Feng, X. D.; Xia, Q.; Yuan, L.; Huang, H. F.; Yang, X. D.; Wang, K. Gadolinium Triggers Unfolded Protein Responses (UPRs) in Primary Cultured Rat Cortical Astrocytes via Promotion of an Influx of Extracellular Ca^{2+} . *Cell Biol. Toxicol.* **2011**, *27*, 1–12.
- Saidak, Z.; Brazier, M.; Kamel, S.; Mentaverri, R. Agonists and Allosteric Modulators of the Calcium-Sensing Receptor and Their Therapeutic Applications. *Mol. Pharmacol.* **2009**, *76*, 1131–1144.
- Brown, E. M. The Calcium-Sensing Receptor: Physiology, Pathophysiology and Car-Based Therapeutics. *Subcell. Biochem.* **2007**, *45*, 139–167.
- Vinken, M. The Adverse Outcome Pathway Concept: a Pragmatic Tool in Toxicology. *Toxicology* **2013**, *312*, 158–165.
- Morcos, S. Nephrogenic Systemic Fibrosis Following the Administration of Extracellular Gadolinium Based Contrast

- Agents: Is the Stability of the Contrast Agent Molecule an Important Factor in the Pathogenesis of This Condition? *Br. J. Radiol.* **2007**, *80*, 73–76.
39. Huang, C.-H.; Nwe, K.; Al Zaki, A.; Brechbiel, M. W.; Tsourkas, A. Biodegradable Polydisulfide Dendrimer Nanoclusters as MRI Contrast Agents. *ACS Nano* **2012**, *6*, 9416–9424.
40. Song, X.; Gong, H.; Yin, S.; Cheng, L.; Wang, C.; Li, Z.; Li, Y.; Wang, X.; Liu, G.; Liu, Z. Cancer Theranostics: Ultra-Small Iron Oxide Doped Polypyrrole Nanoparticles for *in Vivo* Multimodal Imaging Guided Photothermal Therapy. *Adv. Funct. Mater.* **2014**, *24*, 1193–1193.
41. Yu, J.; Yin, W.; Zheng, X.; Tian, G.; Zhang, X.; Bao, T.; Dong, X.; Wang, Z.; Gu, Z.; Ma, X.; *et al.* Smart $\text{MoS}_2/\text{Fe}_3\text{O}_4$ Nanotheranostic for Magnetically Targeted Photothermal Therapy Guided by Magnetic Resonance/Photoacoustic Imaging. *Theranostics* **2015**, *5*, 931–945.
42. Oh, K. Y.; Roberts, V. H.; Schabel, M. C.; Grove, K. L.; Woods, M.; Frias, A. E. Gadolinium Chelate Contrast Material in Pregnancy: Fetal Biodistribution in the Nonhuman Primate. *Radiology* **2015**, *276*, 141488.
43. Kindberg, G. M.; Uran, S.; Frisk, G.; Martinsen, I.; Skotland, T. The Fate of Gd and Chelate Following Intravenous Injection of Gadodiamide in Rats. *Eur. Radiol.* **2010**, *20*, 1636–1643.
44. Huang, M.; Huang, Z. L.; Bilgen, M.; Berkland, C. Magnetic Resonance Imaging of Contrast-Enhanced Polyelectrolyte Complexes. *Nanomedicine* **2008**, *4*, 30–40.
45. De Sousa, P. L.; Livramento, J. B.; Helm, L.; Merbach, A. E.; Meme, W.; Doan, B. T.; Beloile, J. C.; Prata, M. I.; Santos, A. C.; Geraldes, C. F.; *et al.* *In Vivo* MRI Assessment of a Novel Gd³⁺-Based Contrast Agent Designed for High Magnetic Field Applications. *Contrast Media Mol. Imaging* **2008**, *3*, 78–85.
46. Vogt, C.; Pernemalm, M.; Kohonen, P.; Laurent, S.; Hultenby, K.; Vahter, M.; Lehtio, J.; Toprak, M. S.; Fadhel, B. Proteomics Analysis Reveals Distinct Corona Composition on Magnetic Nanoparticles with Different Surface Coatings: Implications for Interactions with Primary Human Macrophages. *PLoS One* **2015**, *10*, e0129008.
47. Yin, H.; Chen, R.; Casey, P. S.; Ke, P. C.; Davis, T. P.; Chen, C. Reducing the Cytotoxicity of ZnO Nanoparticles by a Pre-Formed Protein Corona in a Supplemented Cell Culture Medium. *RSC Adv.* **2015**, *5*, 73963.
48. Cheng, X.; Tian, X.; Wu, A.; Li, J.; Tian, J.; Chong, Y.; Chai, Z.; Zhao, Y.; Chen, C.; Ge, C. Protein Corona Influences Cellular Uptake of Gold Nanoparticles by Phagocytic and Non-phagocytic Cells in a Size-Dependent Manner. *ACS Appl. Mater. Interfaces* **2015**, *7*, 20568–20575.
49. Wang, F.; Yu, L.; Monopoli, M. P.; Sandin, P.; Mahon, E.; Salvati, A.; Dawson, K. A. The Biomolecular Corona is Retained During Nanoparticle Uptake and Protects the Cells From the Damage Induced by Cationic Nanoparticles Until Degraded in the Lysosomes. *Nanomedicine* **2013**, *9*, 1159–1168.
50. Van Schadewijk, A.; Van't Wout, E. F.; Stolk, J.; Hiemstra, P. S. A Quantitative Method for Detection of Spliced X-Box Binding Protein-1 (XBP1) mRNA as a Measure of Endoplasmic Reticulum (ER) Stress. *Cell Stress Chaperones* **2012**, *17*, 275–279.
51. Riedl, S. J.; Shi, Y. Molecular Mechanisms of Caspase Regulation During Apoptosis. *Nat. Rev. Mol. Cell Biol.* **2004**, *5*, 897–907.
52. Kedziorek, D. A.; Muja, N.; Walczak, P.; Ruiz-Cabello, J.; Gilad, A. A.; Jie, C. C.; Bulte, J. W. Gene Expression Profiling Reveals Early Cellular Responses to Intracellular Magnetic Labeling with Superparamagnetic Iron Oxide Nanoparticles. *Magn. Reson. Med.* **2010**, *63*, 1031–1043.
53. Bulte, J. W. *In Vivo* MRI Cell Tracking: Clinical Studies. *AJR, Am. J. Roentgenol.* **2009**, *193*, 314.
54. Chen, Y.-C.; Hsiao, J.-K.; Liu, H.-M.; Lai, I.-Y.; Yao, M.; Hsu, S.-C.; Ko, B.-S.; Chen, Y.-C.; Yang, C.-S.; Huang, D.-M. The Inhibitory Effect of Superparamagnetic Iron Oxide Nanoparticle (Ferucarbotran) on Osteogenic Differentiation and Its Signaling Mechanism in Human Mesenchymal Stem Cells. *Toxicol. Appl. Pharmacol.* **2010**, *245*, 272–279.
55. Liu, Y.; Xia, Q.; Liu, Y.; Zhang, S.; Cheng, F.; Zhong, Z.; Wang, L.; Li, H.; Xiao, K. Genotoxicity Assessment of Magnetic Iron Oxide Nanoparticles with Different Particle Sizes and Surface Coatings. *Nanotechnology* **2014**, *25*, 425101.
56. Sanganeria, P.; Sachar, S.; Chandra, S.; Bahadur, D.; Ray, P.; Khanna, A. Cellular Internalization and Detailed Toxicity Analysis of Protein-Immobilized Iron Oxide Nanoparticles. *J. Biomed. Mater. Res., Part B* **2015**, *103*, 125–134.
57. Coburger, J.; Engelke, J.; Scheuerle, A.; Thal, D. R.; Hlavac, M.; Wirtz, C. R.; König, R. Tumor Detection with 5-Aminolevulinic Acid Fluorescence and Gd-DTPA-Enhanced Intraoperative MRI at the Border of Contrast-Enhancing Lesions: a Prospective Study Based on Histopathological Assessment. *Neurosurg. Focus* **2014**, *36*, E3.
58. Nel, A.; Xia, T.; Meng, H.; Wang, X.; Lin, S.; Ji, Z.; Zhang, H. Nanomaterial Toxicity Testing in the 21st Century: Use of a Predictive Toxicological Approach and High-Throughput Screening. *Acc. Chem. Res.* **2013**, *46*, 607–621.
59. Mbeh, D. A.; Mireles, L. K.; Stanicki, D.; Tabet, L.; Maghni, K.; Laurent, S.; Sacher, E.; Yahia, L. Human Alveolar Epithelial Cell Responses to Core-Shell Superparamagnetic Iron Oxide Nanoparticles (Spions). *Langmuir* **2015**, *31*, 3829–3839.
60. Wydra, R. J.; Rychahou, P. G.; Evers, B. M.; Anderson, K. W.; Dziubla, T. D.; Hilt, J. Z. The Role of ROS Generation from Magnetic Nanoparticles in an Alternating Magnetic Field on Cytotoxicity. *Acta Biomater.* **2015**, *25*, 284–290.
61. Torrisi, V.; Graillot, A.; Vitorazi, L.; Crouzet, Q.; Marletta, G.; Loubat, C.; Berret, J. F. Preventing Corona Effects: Multi-phosphonic Acid Poly(Ethylene Glycol) Copolymers for Stable Stealth Iron Oxide Nanoparticles. *Biomacromolecules* **2014**, *15*, 3171–3179.
62. Blazak, W. F.; Brown, G. L.; Gray, T. J.; Treinen, K. A.; Denny, K. H. Developmental Toxicity Study of Mangafodipir Tri-sodium Injection (Mndpdip) in New Zealand White Rabbits. *Toxicol. Sci.* **1996**, *33*, 11–15.
63. O'Neal, S. L.; Zheng, W. Manganese Toxicity Upon Overexposure: a Decade in Review. *Curr. Environ. Health Rep.* **2015**, *2*, 315–328.
64. Crossgrove, J.; Zheng, W. Manganese Toxicity upon Overexposure. *NMR Biomed.* **2004**, *17*, 544–553.
65. Kumar, V.; Abbas, K. A.; Aster, J. *Robbins Basic Pathology*, 9th ed.; Saunders/Elsevier: Amsterdam, 2012.